Journal of Fluorescence
https://doi.org/10.1007/s10895-020-02502-5

ORIGINAL ARTICLE

A Visual FRET Immunofluorescent Biosensor for Ratiometric Parathyroid Hormone (1–84) Antigen Point-of-Care Detection

Yixin Nie [1,2] · Jingting Li [1,2] · Yang Liu [1,2] · Qian Zhang [1,2] · Qiang Ma [1,2]

Received: 30 December 2019 / Accepted: 27 January 2020

Abstract

Excessive secretion of PTH leads to disturbance of calcium and phosphorus metabolism in the body, which promotes bone, kidney, digestive system and nervous system diseases. Due to the short half-life of PTH, it becomes a difficult issue for PTH detection in the clinical diagnosis field. We explored a competitive immunofluorescent sensing mode based on FRET of two-color CdTe QDs for ratiometric PTH 1–84 antigen detection. The FRET effect and ratiometric fluorescence between the two-color CdTe QDs motivated accurate quantification of PTH 1–84 antigen concentration from 0.01 ng mL^{-1} to 0.08 ng mL^{-1} with a limit of detection of 3 pg mL^{-1}. More importantly, under UV irradiation, samples with different concentrations of PTH 1–84 antigen achieved fluorescence visualization, which provides huge possibility for the practical application of PTH 1–84 antigen point-of-care detection.

Keywords Ratiometric fluorescence · PTH 1–84 antigen determination · FRET · Fluorescence visualization

Abbreviation

PTH	parathyroid hormone
FRET	Forster resonance energy transfer
CdTe QDs	CdTe quantum dots
cAMP	cyclic adenosine monophosphate
POC	point-of-care
MPA	3-mercaptopropionic acid
PDDA	poly dimethyl diallyl ammonium chloride
EDC	1-(3-dimethylaminopropyl)-3-ethylcarbodiimide hydrochloride
NHS	N-hydroxysuccinimide
PL	photoluminescence
TEM	transmission electron microscopy
UV-vis	ultraviolet-visible
FT-IR	Fourier transform infrared spectrometry

Introduction

PTH is a basic single-chain peptide hormone composed of 84 amino acids secreted by the parathyroid primary cells [1], which regulates the metabolism of calcium and phosphorus in vertebrates and excites a variety of intracellular signals from cAMP and protein kinases A and C [2, 3]. In addition, the level of PTH also reflects the severity of cardiovascular disease, chronic kidney disease, and some types of cancer (such as breast cancer and prostate cancer). In general, determination of PTH in human blood is of great significance for monitoring parathyroid disease, osteoporosis, and malignant hypercalcemia [4]. Meanwhile, in thyroidectomy, the parathyroid glands are often mistakenly removed, resulting in the lack of PTH in the human body, which leads to a series of sequelae such as calcium deficiency in patients after surgery. Therefore, it is also especially necessary to avoid the removal of the parathyroid glands based on the secretion of PTH during surgery. As of today, only a few methods, including fluorescence, chromatography and electrochemical analysis, have explored PTH detection [1–3, 5–7]. However, due to the short half-life of PTH (only a few minutes) [7], exploring a fast and accurate method is still an essential issue.

POC is a fast and accurate modern detection method emerging in the field of clinical diagnosis [8]. It has unique advantages, for example: it can be operated by non-professionals [9], simple and efficient, small and easy to store, especially suitable for areas with limited medical resources [10], and consumes low energy [11]. Therefore, POC-based

✉ Qiang Ma
Qma@jlu.edu.cn

[1] Department of Analytical Chemistry, College of Chemistry, Jilin University, Changchun 130012, China

[2] National Chemistry Experimental Teaching Demonstration Center, Jilin University, Changchun 130012, China

Published online: 04 February 2020

diagnosis is now a key tool for reducing disease incidence and mortality [12]. Therefore, major organizations around the world (US Global Health Action Plan, UK Department for International Development, etc.) are conducting research and development for POC [10]. Among the many manifestations of POC, fluorescence visualization has become one of the most intuitive forms. We can accurately determine the level of measurement results through intuitive color changes.

In the work (as shown in Scheme 1), we applied the FRET effect between two-color CdTe QDs for ratiometric PTH 1–84 antigen detection with competitive immunofluorescent sensing. First, the green CdTe QDs attached to the PTH 1–84 antibody were overlaid on the glass slide. The antibody then was combined with the target antigen. Finally, the PTH 1–84 antigen linked to the red CdTe QDs competed with the target antigen for binding to the PTH 1–84 antibody on the glass slide, which caused FRET effect between the two-color CdTe QDs, resulting in an increase in green light intensity and a decrease in red light intensity. Therefore, a simple and efficient sensing mode for accurate ratiometric quantification of PTH 1–84 antigen concentration has been pioneered. Most importantly, as the concentration of the PTH 1–84 antigen changed, the color of the samples under UV light gradually changed, indicating the great practical potential in the clinical detection of PTH 1–84 antigen.

Materials and Methods

Reagents and Apparatus

All chemical reagents in this experiment were of analytical grade. NaOH, $NaBH_4$, MPA, strontium powder, $CdCl_2$, 20% mass fraction of PDDA, PTH 1–84 antigen, PTH 1–84 antibody, EDC, and NHS were purchased from Sangon Biotech Co., Ltd. (Shanghai, China). All reagents were produced by ultrapure water with resistivity of greater than 18 MΩ cm^{-1}. Human serum was acquired as the gift from Third Hospital of Jilin University. All experiments were carried out under room temperature.

PL spectra measurements were achieved on a Shimadzu RF-5301 PC spectrofluorophotometer (Shimadzu Co., Kyoto, Japan). TEM images were performed by a Hitachi electron microscope operating at a 200 kV acceleration voltage. The ultraviolet-visible (UV-vis) absorption spectra were obtained on a Varian GBC Cintra 10e UV-vis spectrometer with a 1 cm quart cell. FT-IR was taken on a Thermo Nicolet 360 FTIR spectrometer using KBr pellets. All pH measurements were achieved with a PHS-3C pH meter (Tuopu Co., Hangzhou, China).

Preparation of CdTe QDs

0.1276 g of cerium powder and 0.080 g of $NaBH_4$ were dissolved in 3 mL of ultrapure water, and the reaction was carried out under 0 °C with magnetic stirring. During the reaction, the system was contacted with atmosphere through a needle. The white turbid liquid was acquired after 4 h. After standing for 10 min, an upper layer of a colorless aqueous solution of NaHTe was obtained. CdTe QDs were produced by hydrothermal reflux. First, 1.25 mmol mL^{-1} $CdCl_2$ solution was prepared with nitrogen purification, and the pH of the solution was adjusted to 11. Then, the fresh NaHTe solution was injected into the $CdCl_2$ solution. The solution was refluxed at 100 °C under stirring. By controlling the heating time,

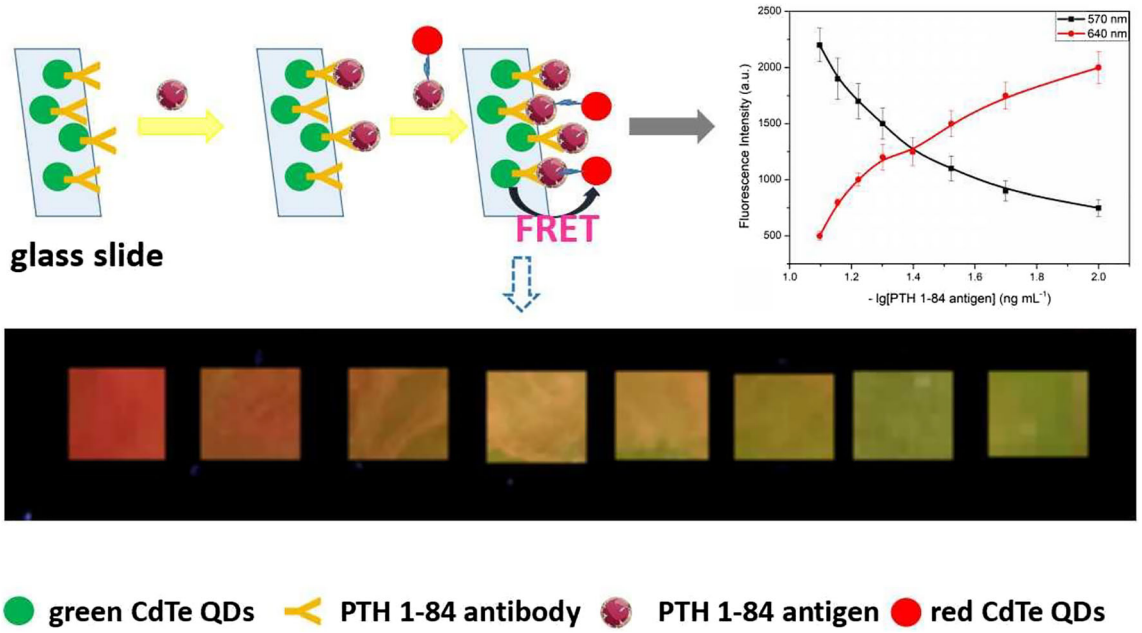

Scheme 1 Schematic diagram of competitive immune sensing mode.

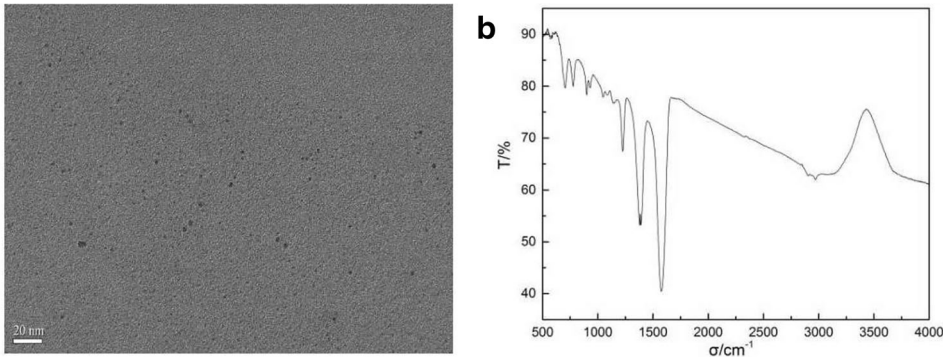

Fig. 1 (A) TEM image and (B) FT-IR spectrum of CdTe QDs

CdTe QDs with different suitable sizes were synthesized. The green CdTe QDs were first obtained when solution was discharged from the condenser after heating for 1 h. And the red CdTe QDs were achieved after 2 h.

Preparation of CdTe QD@PTH 1–84 Antigen and CdTe QD@PTH 1–84 Antibody

0.01 mmol of EDC and NHS was added to 50 μL of 20 μg mL^{-1} PTH 1–84 antigen solution, respectively. Then the red CdTe QDs solution was mixed in the solution to 2 mL. After incubating for 2 h in the dark, the CdTe QD@PTH 1–84 antigen was prepared. The glass slide was immersed in the diluted PDDA solution for 30 min and dried. Next, it was immersed in the green CdTe QDs solution for 30 min and dried. Finally, it was immersed in the diluted PTH 1–84 antibody solution for 30 min and dried to acquire the glass slide with green CdTe QD@PTH 1–84 antibody conjugate.

Visual Immunofluorescent Analysis

The above-mentioned glass slide with the green CdTe QD@PTH 1–84 antibody conjugate was immersed in standard solution containing the target antigen for 30 min and then dried. It was then immersed in CdTe QD@PTH 1–84 antigen solution for 30 min and dried. Finally, the measurements of fluorescence intensity of the glass slide was carried out.

Results and Discussion

Characterization of CdTe QDs

As shown in the TEM image of CdTe QDs (Fig. 1A), particles have good dispersibility and uniform size with the average particle size is about 2 nm. From the FT-IR spectrum (Fig. 1B) of the CdTe QDs, both the peak of S-H at about 2550 cm^{-1} and the vibration absorption peaks of C=O at about 1700 cm^{-1} in carboxylic acid molecule cannot be observed. But two carboxylic acid-like peaks appear at 1558 cm^{-1} and 1395 cm^{-1}. It indicates that mercapto group and carboxyl group in MPA coordinates with Cd^{2+} on the surface of the QDs. As we all known, reduction of surface defects of QDs leads to increase of fluorescent efficiency. Surface defects as the non-radiative recombination centers in CdTe QDs can be filled due to coordination of MPA, which improves the stability and luminescence intensity of CdTe QDs [13, 14]. Figure 2 shows the UV-visible absorption spectrum and fluorescence spectrum of CdTe QDs prepared from different reaction time. The lowest excitation energy is indicated by the first visible peak on the right side of the absorption spectrum, which is called the first exciton absorption peak, also known as the quantum confinement peak. The first exciton absorption peak corresponds to the 1 s–1 s orbital transition of electrons in CdTe QDs. The appearance of the peak exhibits that the electronic energy level of CdTe QDs has been transformed into a discrete energy level structure with molecular characteristics, and is no longer a quasi-continuous structure of the bulk phase. When the heating time is 60 min (curve a), the absorption spectrum exhibits a distinct structural peak, indicating that the reaction solution produces CdTe nanocrystals and

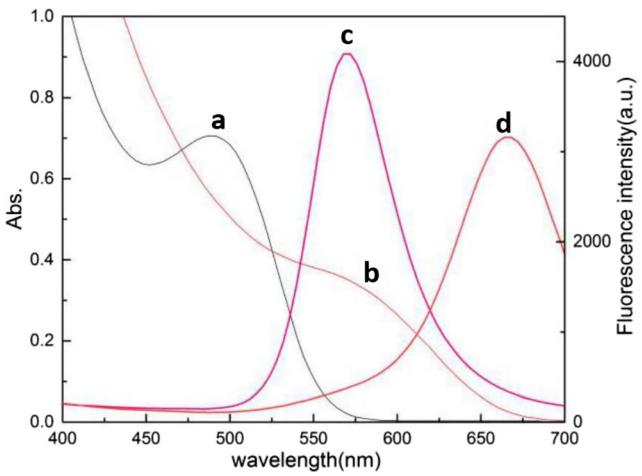

Fig. 2 UV-visible absorption spectrum and fluorescence spectrum of CdTe QDs: (a) absorption spectrum of heating time of 60 min; (b) absorption spectrum of heating time of 120 min; (c) fluorescence spectrum of heating time of 60 min; (d) fluorescence spectrum of heating time of 120 min

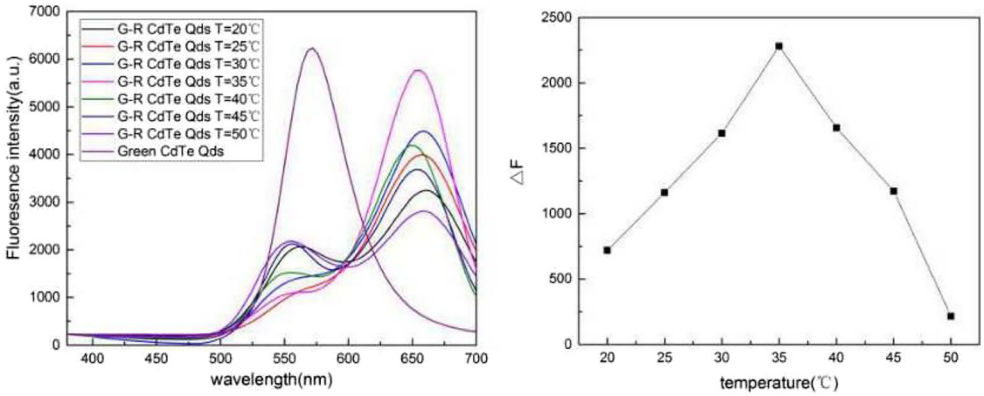

Fig. 3 Optimization of reaction temperature in CdTe QDs synthesis

1 s–1 s electronic transition. As the reaction time prolongs, the absorption spectrum of CdTe QDs solution gradually shifts to the long wavelength direction, gradually shifting from 500 nm (60 min) to 600 nm (120 min, curve b), and the absorption peak is gradually broadened and structured, which turns into a shoulder peak. This indicates that the particle size of CdTe QDs in the system is gradually increased and non-uniform with wider particle size distribution. From the fluorescence spectrum of CdTe QDs, when the reaction time is 60 min (curve c), since the small particle size of CdTe QDs, the fluorescence emission peak conforms to Gaussian distribution with narrow half-width and good symmetry. With the extension of reaction time, the fluorescence emission spectrum of CdTe QDs red-shifts from 560 nm (60 min) to 660 nm (120 min, curve d), and the half-width of the fluorescence emission spectrum also increases. With the increased particle size of QDs and the decreased specific surface area [15, 16], the binding effect of the passivated surface and absorbed light energy reduce. So that the absorption spectrum is red-shifted and the corresponding fluorescence emission peak wavelength is also red-shifted.

Condition Optimization Experiment

The fluorescence of the glass slide was detected at room temperature (25 °C) (excitation and emission wavelengths were 360 nm and 380 nm, respectively). As shown in Fig. 3, when the immune reaction temperature was 35 °C, the fluorescence intensity was the highest, so 35 °C was selected as the optimum temperature for the immune reaction.

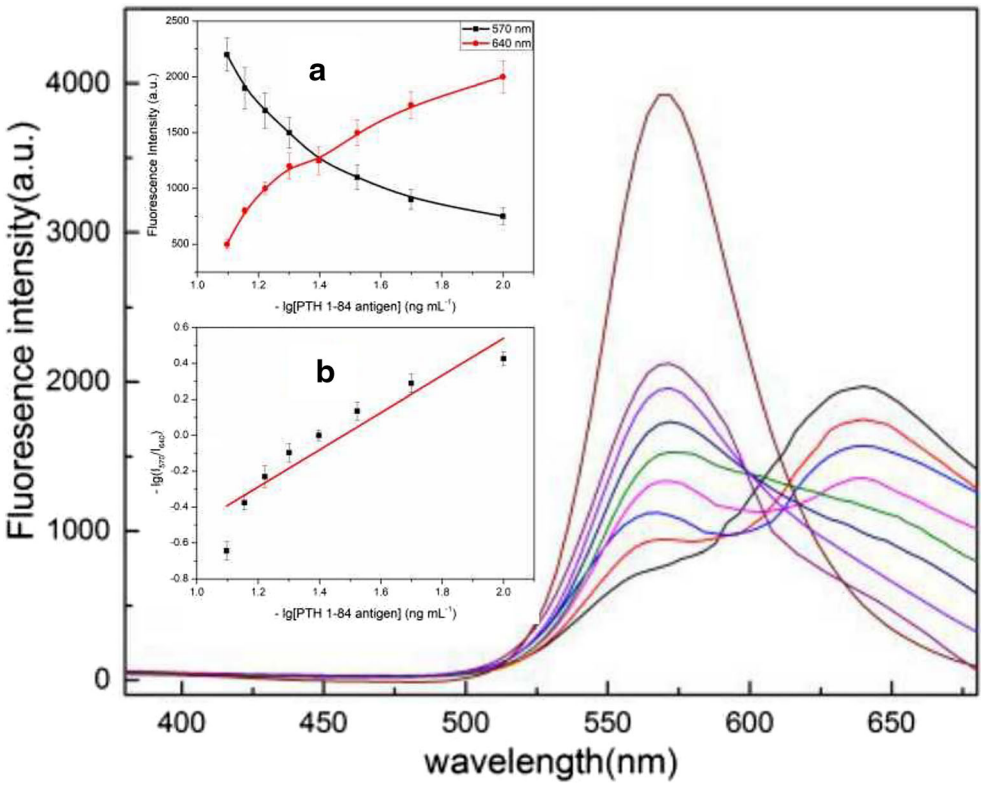

Fig. 4 FL intensity of the sensor at 570 nm and 640 nm with different concentrations of PTH 1–84 antigen from 0.01 to 0.08 ng mL^{-1}. (insert: (A) relationship between fluorescence intensity of the sensor with different concentrations of PTH 1–84 antigen. (B) Calibration curve for quantification of PTH 1–84 antigen)

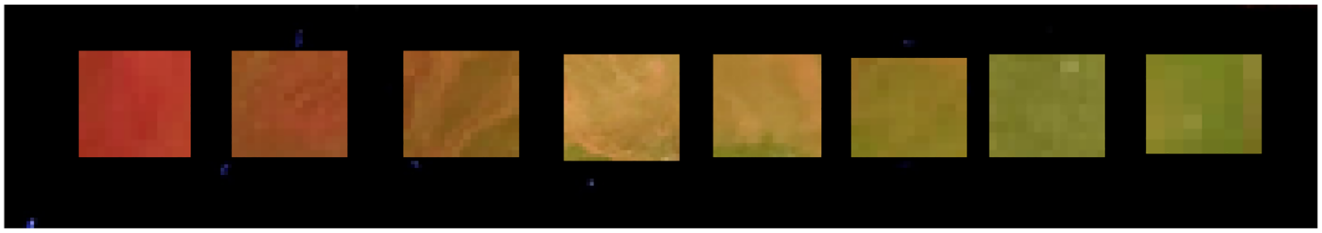

Fig. 5 Photos of the glass slide with different concentrations of PTH 1–84 antigen under UV light

Table 1 Results for determination of PTH 1–84 antigen in the real samples

S	Add (ng mL^{-1})	Found ($molL^{-1}$)	Recovery (%)	RSD (%, $n = 3$)
1	0.01	0.0108	108	3.84
2	0.05	0.0525	105	4.21
3	0.08	0.0808	101	3.25

PTH 1–84 Antigen Determination

Figure 4 below exhibits the fluorescence spectra of the competitive immune recognition system in the presence of standard solutions with different PTH 1–84 antigen concentrations. As shown, when the target antigen concentration gradually increases, the concentration of CdTe QD@PTH 1–84 antigen that competes for binding to the antibody decreased, so that FRET between the red CdTe QDs and the green CdTe QDs reduces, resulting in an increase in green light intensity and a decrease in red light intensity. As exhibited in Fig. 4 (insert A, B), the linear equation between lg[PTH 1–84 antigen] and $lg(I_{570}/I_{640})$ was $lg(I_{570}/I_{640}) = 1.0348$ lg[PTH 1–84 antigen] + 1.529 with an LOD of 3 pg mL^{-1}. According to previous formula [17, 18]:

$$R_0 = 0.0211\left[k^2\Phi_D(n)^{-4}J(\lambda)\right]^{1/6}$$

$$\Phi_{ET} = \frac{1}{1+\left(\frac{d}{d_o}\right)^n}$$

R_0 is Förster distance, κ^2 is orientation factor (2/3) [19, 20], Φ_D is the quantum yield of CdTe QDs, n is the refractive index of water, J(λ) is the overlap integral of fluorescence spectrum and molar absorption spectrum, Φ_{ET} is energy transfer efficiency, d is real distance.

The value of d is calculated as 5.49 nm, which proves that the form of energy transfer in the system is FRET. Moreover, under the UV light, when the concentration of PTH 1–84 antigen in the standard solution increases from 0.01 to 0.03 ng mL^{-1}, the color of the glass slide gradually changes from red to orange (as exhibited in Fig. 5). When the concentration is between 0.04 and 0.05 ng mL^{-1}, the color becomes yellow. And it can generally become green when the antigen concentration achieves 0.06–0.08 ng mL^{-1}. In order to further evaluate the robustness of the method for the analysis of actual serum samples, a recovery experiment with standard addition method was performed (Table 1). The recovery is defined as the ratio of the detected target concentration (based on the linear equation) to the added target concentration in the sample. The standard solution containing PTH 1–84 antigen with different concentrations was prepared by using 20 times diluted human serum instead of deionized water, and each experiment was carried out for 3 times. As a result, the calculated recovery rate is satisfactory. In addition, the determination system we explored has higher sensitivity than other methods (Table 2), and the linear range covers clinically tested normal value (0.07 ng mL^{-1}), which achieves the value of clinical application.

Conclusions

The 2-mercaptopropionic acid stabilized two-color CdTe QDs synthesized by hydrothermal method have excellent

Table 2 Comparison with other sensing methods

Methods	The linear range	LOD	References
EONs-based ECL sensor	0.05–8 ng mL^{-1}	0.017 ng mL^{-1}	Maldaner [21]
Electrochemical immunosensor	10–50 pg mL^{-1}	7.65 pg mL^{-1}	Sayikli Şimşek [1]
Electrochemical immunosensor	50–500 ng mL^{-1}		Espinoza-Castañeda [2]
Nanoporous membrane	60–400 ng mL^{-1}	55 ng mL^{-1}	Escosura-Muñiz [5]
Acoustic wave biosensor	0.061–100 μg mL^{-1}	61 ng mL^{-1}	Crivianu-Gaita [3]
Capillary zone electrophoresis method	0.25–250 μg mL^{-1}	0.25 μg mL^{-1}	Li [4]
Two-color CdTe QDs sensor	0.01–0.08 ng mL^{-1}	3 pg mL^{-1}	This work

luminescent properties. On the glass slide, PTH 1–84 antigen linked with red CdTe QDs are immunocompetently bound to the PTH 1–84 antibody connected to the green CdTe QDs. Eventually, as the concentration of the PTH 1–84 antigen increases, the green fluorescent signal gradually increases while the red fluorescent signal gradually decreases, which achieves ratiometric fluorescence. Excitingly, under the irradiation of UV light, with the increasing concentration of PTH 1–84 antigen, the color on the glass piece gradually changes from red to green. In our future work, higher sensitive QD-based sensing system is expected to overcome the actual limitation about the large serum dilution multiples in sample testing. In summary, the simple pattern with obvious phenomena have greatly increased the potential of the work for point-of-care determination.

Acknowledgements The authors gratefully acknowledge financial support from the Youth Science Fund of Jilin Province (20140520081JH) and the "Thirteenth Five Year" Project of the Science and Technology Research in the Education Department of Jilin Province, China.

References

1. Sayikli Şimşek C, Nur Sonuç Karabo a M, Sezgintürk MK (2015) A new immobilization procedure for development of an electrochemical immunosensor for parathyroid hormone detection based on gold electrodes modified with 6-mercaptohexanol and Silane. Talanta 144:210–218
2. Espinoza-Castañeda M, Escosura-Muñiz A, Chamorro A, Torres C, Merkoçi A (2015) Nanochannel array device operating through Prussian blue nanoparticles for sensitive label-free immunodetection of a cancer biomarker. Biosens Bioelectron 67: 107–114
3. Crivianu-Gaita V, Aamer M, Posaratnanathan RT, Romaschin A, Thompson M (2016) Acoustic wave biosensor for the detection of the breast and prostate cancer metastasis biomarker protein PTHrP. Biosens Bioelectron 78:92–99
4. Li S, Liu Y, Ma Q (2019) A novel polydopamine electrochemiluminescence organic nanoparticlebased biosensor for parathyroid hormone detection. Talanta 202:540–545
5. Escosura-Muñiz A, Espinoza-Castañeda M, Chamorro-García A, RodríguezHernández CJ, Torres C, Merkoçi A (2018) In situ monitoring of PTHLH secretion in neuroblastoma cells cultured onto nanoporous membranes. Biosens Bioelectron 107:62–68
6. Otieno BA, Krause CE, Jones AL, Kremer RB, Rusling JF (2016) Cancer diagnostics via ultrasensitive multiplexed detection of parathyroid hormone-related peptides with a microfluidic immunoarray. Anal Chem 88:9269–9275
7. Özcan HM, Yildiz K, Çakar C, Aydin T, Asav E, Sağiroğlu A, Sezgintürk MK (2015) Ultrasensitive impedimetric biosensor fabricated by a new immobilisation technique for parathyroid hormone. Appl Biochem Biotechnol 176:1251–1262
8. Luppa PB, Müller C, Schlichtiger A, Schlebusch H (2011) Point-of-care testing (POCT): current techniques and future perspectives. TrAC Trends Anal Chem 30:887–898
9. Liu JJ, Geng ZX, Fan ZY, Liu J, Chen HD (2019) Point-of-care testing based on smartphone: the current state-of-the-art (2017–2018). Biosens Bioelectron 132:17–37
10. Chan HN, Tan MJA, Wu H (2017) Point-of-care testing: applications of 3D printing. Lab Chip 17:2713–2739
11. Arduini F, Micheli L, Moscone D, Palleschi G, Piermarini S, Ricci F, Volpe G (2016) Electrochemical biosensors based on nanomodified screen-printed electrodes: recent applications in clinical analysis. TrAC Trends Anal Chem 79:114–126
12. Urdea M, Penny LA, Olmsted SS, Giovanni MY, Kaspar P, Shepherd A, Wilson P, Dahl CA, Buchsbaum S, Moeller G, Hay Burgess DC (2006) Requirements for high impact diagnostics in the developing world. Nature 444:73–79
13. Mehta A, Im J, Kim BH, Min H, Nie R, Seok S (2018) Stabilization of Lead–tin-alloyed inorganic–organic halide Perovskite quantum dots. ACS Nano 12:12129–12139
14. Goswami SK, Kim TS, Oh E, Challa KK, Kim ET (2012) Optical properties and effect of carrier tunnelling in CdSe colloidal quantum dots: a comparative study with different ligands. AIP Adv 2: 032132
15. Wei MB, Hong YZ, Han DL, Yang LI, Liu HL, Su LX (2018) One-step hydrothermal synthesis of ZnS quantum dots-reduced Graphene oxide composites with enhanced Photocatalytic activity. Phys Status Solidi A 215:1800082
16. Chen DY, Huang SS, Huang RT, Zhang Q, Le TT, Cheng E, Hu ZJ, Chen ZW (2019) Convenient fabrication of Ni-doped SnO2 quantum dots with improved photodegradation performance for Rhodamine B. J Alloys Compd 788:929–935
17. Chen C, Midelet C, Bhuckory S, Hildebrandt N, Werts MV (2018) Nanosurface energy transfer from long-lifetime terbium donors to gold nanoparticles. J Phys Chem C 122:17566–17574
18. Prajapati R, Chatterjee S, Bhattacharya A, Mukherjee TK (2015) Surfactant-induced modulation of Nanometal surface energy transfer from silicon quantum dots to silver nanoparticles. J Phys Chem C 119:13325–13334
19. Yu XZ, Wen K, Wang ZH, Zhang XY, Li CL, Zhang SX, Shen JZ (2016) General bioluminescence resonance energy transfer homogeneous immunoassay for small molecules based on quantum dots. Anal Chem 88:3512–3520
20. Kotresh MG, Adarsh KS, Shivkumar MA, Mulimani BG, Savadatti MI, Inamdar SR (2015) Spectroscopic investigation of alloyed quantum dot-based FRET to cresyl violet dye. Luminescence. 31: 760–768
21. Maldaner FPS, Perobelli RF, Xavier B, Remuzzi GL, Walter ME, Dalmora SL (2017) Evaluation of recombinant human parathyroid hormone by CZE method and its correlation with in vitro bioassay and LC methods. Talanta 162:567–573